internal solution containing 140 mM KCl, 2 mM $MgCl_2$, 10 mM EGTA, 10 mM HEPES at pH 7.2. The external solution was Leibovitz's L-15 (Gibco) containing 136 mM NaCl, 5.8 mM NaH_2PO_4, 5.4 mM KCl, 1.3 mM $CaCl_2$, 0.9 mM $MgCl_2$ at pH 7.2. Osmolarity was adjusted to 300 mosM l^{-1}. Motility was measured and calibrated using an electro-optical method in which the cell's ciliated pole was imaged through a rectangular slit onto a photodiode[29].

In vivo functional assays

For ABR, DPOAE and CM measurements, mice were anaesthetized with xylazine and ketamine. ABRs and DPOAEs were obtained from one set of animals; CMs from a second set. For ABR, needle electrodes were inserted at vertex and pinna. ABR and CM were evoked with 5-ms tone pips (0.5-ms rise–fall, with a $\cos^2$ envelope, at 35 per s). The response was amplified (× 10,000), filtered (0.1–3 kHz), and averaged with an A/D board in a PC-based data-acquisition system. Sound level was raised in 5-dB steps from 0 to 90 dB SPL. At each level, 1,024 responses were averaged (with stimulus polarity alternated) after 'artefact rejection'. Threshold was determined by visual inspection. For CM a silver-wire electrode was placed on the round window membrane. Responses to alternating pip polarities were subtracted, and the resultant waveform was digitally high-pass filtered to remove residual uncancelled neural potentials. The DPOAE at $2f_1 - f_2$ was recorded in response to two primary tones: f_1 and f_2, with $f_2/f_1 = 1.2$ and the f_2 level 10 dB lower than the f_1 level. Ear-canal sound pressure was amplified and digitally sampled at 4-μs intervals. Fast-Fourier transforms were computed from averaged waveforms of ear-canal sound pressure, and the DPOAE amplitude at $2f_1 - f_2$ and surrounding noise floor were extracted. Iso-response contours were interpolated from plots of amplitude versus sound level, performed in 5-dB steps of f_1 level. Threshold is defined as the f_1 level required to produce a DPOAE at 0 dB SPL.

Received 29 May; accepted 12 August 2002; doi:10.1038/nature01059.
Published online 28 August 2002.

1. Gold, T. Hearing. II. The physical basis of the action of the cochlea. *Proc. R. Soc. Lond. B* **135,** 492–498 (1948).
2. Dallos, P. & Harris, D. Properties of auditory nerve responses in absence of outer hair cells. *J. Neurophysiol.* **41,** 365–383 (1978).
3. Brown, M. C., Nuttall, A. L. & Masta, R. I. Intracellular recordings from cochlear inner hair cells: effects of stimulation of the crossed olivocochlear efferents. *Science* **222,** 69–72 (1983).
4. Dallos, P. The active cochlea. *J. Neurosci.* **12,** 4575–4585 (1992).
5. Brownell, W. E., Bader, C. R., Bertrand, D. & de Ribaupierre, Y. Evoked mechanical responses of isolated cochlear outer hair cells. *Science* **227,** 194–196 (1985).
6. Kachar, B., Brownell, W. E., Altschuler, R. & Fex, J. Electrokinetic shape changes of cochlear outer hair cells. *Nature* **322,** 365–368 (1986).
7. Ashmore, J. F. A fast motile response in guinea-pig outer hair cells: the cellular basis of the cochlear amplifier. *J. Physiol.* **388,** 323–347 (1987).
8. Ashmore, J. F. *Cochlear Mechanisms* (eds Wilson, J. P. & Kemp, D. T.) 107–116 (Plenum, London, 1989).
9. Santos-Sacchi, J. Reversible inhibition of voltage-dependent outer hair cell motility and capacitance. *J. Neurosci.* **11,** 3096–3110 (1991).
10. Zheng, J. *et al.* Prestin is the motor protein of cochlear outer hair cells. *Nature* **405,** 149–155 (2000).
11. Belyantseva, I. A., Adler, H. J., Curi, R., Frolenkov, G. I. & Kachar, B. Expression and localization of prestin and the sugar transporter GLUT-5 during development of electromotility in cochlear outer hair cells. *J. Neurosci.* **20,** RC116 (2000).
12. Oliver, D. *et al.* Intracellular anions as the voltage sensor of prestin, the outer hair cell motor protein. *Science* **292,** 2340–2343 (2001).
13. Forge, A. Structural features of the lateral walls in mammalian cochlear outer hair cells. *Cell Tissue Res.* **265,** 473–483 (1991).
14. Dallos, P. & Fakler, B. Prestin, a new type of motor protein. *Nature Rev. Mol. Cell Biol.* **3,** 104–111 (2002).
15. Bohne, B. A. & Rabbitt, K. D. Holes in the reticular lamina after noise exposure: implication for continuing damage in the organ of Corti. *Hear. Res.* **11,** 41–53 (1983).
16. Holt, J. R. *et al.* A chemical-genetic strategy implicates myosin-1c in adaptation by hair cells. *Cell* **108,** 371–381 (2002).
17. Kros, C. J. *et al.* Reduced climbing and increased slipping adaptation in cochlear hair cells of mice with Myo7a mutations. *Nature Neurosci.* **5,** 41–47 (2002).
18. Dallos, P. & Wang, C. Y. Bioelectric correlates of kanamycin intoxication. *Audiology* **13,** 277–289 (1974).
19. Kemp, D. T. Stimulated acoustic emissions from within the human auditory system. *J. Acoust. Soc. Am.* **64,** 1386–1391 (1978).
20. Johnstone, B. M., Patuzzi, R. & Yates, G. K. Basilar membrane measurements and the travelling wave. *Hear. Res.* **22,** 147–153 (1986).
21. Ruggero, M. A. & Rich, N. C. Application of a commercially-manufactured Doppler-shift laser velocimeter to the measurement of basilar-membrane vibration. *Hear. Res.* **51,** 215–230 (1991).
22. Sellick, P. M., Patuzzi, R. & Johnstone, B. M. Measurement of basilar membrane motion in the guinea pig using the Mossbauer technique. *J. Acoust. Soc. Am.* **72,** 131–141 (1982).
23. Kiang, N. Y. & Moxon, E. C. Tails of tuning curves of auditory-nerve fibers. *J. Acoust. Soc. Am.* **55,** 620–630 (1974).
24. Ruggero, M. A. Responses to sound of the basilar membrane of the mammalian cochlea. *Curr. Opin. Neurobiol.* **2,** 449–456 (1992).
25. Manley, G. A. Cochlear mechanisms from a phylogenetic viewpoint. *Proc. Natl Acad. Sci. USA* **97,** 11736–11743 (2000).
26. Fettiplace, R., Ricci, A. J. & Hackney, C. M. Clues to the cochlear amplifier from the turtle ear. *Trends Neurosci.* **24,** 169–175 (2001).
27. Hudspeth, A. J. Mechanical amplification of stimuli by hair cells. *Curr. Opin. Neurobiol.* **7,** 480–486 (1997).
28. Ehret, G. *The Auditory Psychobiology of the Mouse* (ed. Willott, J. F.)) 169–200 (Charles Thomas, Springfield, Illinois, 1983).
29. He, D. Z., Evans, B. N. & Dallos, P. First appearance and development of electromotility in neonatal gerbil outer hair cells. *Hear. Res.* **78,** 77–90 (1994).

Acknowledgements

We thank K. Cullen for technical assistance; T. Curran, B. Fritzsch, C. A. Shera and D. Freeman for comments on the manuscript; and B. Kachar, T. Hasson and P. Gillespie for antibodies. This work is supported in part by NIH grants to M.C.L., Z.Z.H. and J.Z., NIH Cancer Center Support CORE grant, and the American Lebanese Syrian Associated Charities (ALSAC).

Competing interests statement

The authors declare that they have no competing financial interests.

Correspondence and requests for materials should be addressed to J.Z. (e-mail: jian.zuo@stjude.org).

Robustness of the BMP morphogen gradient in *Drosophila* embryonic patterning

Avigdor Eldar*†, Ruslan Dorfman*, Daniel Weiss*†, Hilary Ashe‡, Ben-Zion Shilo* & Naama Barkai*†

** Department of Molecular Genetics and † Department of Physics of Complex Systems, Weizmann Institute of Science, Rehovot, Israel*
‡ School of Biological Sciences, University of Manchester, Manchester M13 9PT, UK

Developmental patterning relies on morphogen gradients, which generally involve feedback loops to buffer against perturbations caused by fluctuations in gene dosage and expression[1]. Although many gene components involved in such feedback loops have been identified, how they work together to generate a robust pattern remains unclear. Here we study the network of extracellular proteins that patterns the dorsal region of the *Drosophila* embryo by establishing a graded activation of the bone morphogenic protein (BMP) pathway. We find that the BMP activation gradient itself is robust to changes in gene dosage. Computational search for networks that support robustness shows that transport of the BMP class ligands (Scw and Dpp) into the dorsal midline by the BMP inhibitor Sog is the key event in this patterning process. The mechanism underlying robustness relies on the ability to store an excess of signalling molecules in a restricted spatial domain where Sog is largely absent. It requires extensive diffusion of the BMP–Sog complexes, coupled with restricted diffusion of the free ligands. We show experimentally that Dpp is widely diffusible in the presence of Sog but tightly localized in its absence, thus validating a central prediction of our theoretical study.

Graded activation of the BMP pathway subdivides the dorsal region of *Drosophila* embryos into several distinct domains of gene expression. This graded activation is determined by a well-characterized network of extracellular proteins[2,3], which may diffuse in the perivitelline fluid[4] that surrounds the embryo (Fig. 1a). The patterning network is composed of two BMP class ligands (Scw and Dpp), a BMP inhibitor (Sog), a protease that cleaves Sog (Tld) and an accessory protein (Tsg), all of which are highly conserved in evolution and are used also for patterning the dorso-ventral axis of vertebrate embryos[5]. Previous studies have suggested that patterning of the dorsal region is robust to changes in the concentrations of most of the crucial network components. For example, embryos that contain only one functional allele of *scw*, *sog*, *tld* or *tsg* are viable and do not show any apparent phenotype. Misexpression of *scw* or of *tsg* also renders the corresponding null mutants viable[6–8].

To check whether robustness is achieved at the initial activation gradient, we monitored signalling directly by using antibodies that recognize specifically an activated, phosphorylated intermediate of

the BMP pathway (pMad)[9,10]. Prominent graded activation in the dorsal-most eight cell rows was observed for about 1 h, starting roughly 2 h after fertilization at 25 °C (ref. 11 and Fig. 1b). We quantified this activation gradient in heterozygous mutants that were compromised for one of three of the crucial components of the patterning network, Scw, Sog or Tld. Whereas homozygous null mutants that completely lack the normal gene product have a deleterious effect on signalling[11], the heterozygotes, which should produce half the amount of the gene product, were indistinguishable from wild type (Fig. 1c). Similarly, overexpression of the Tld protein uniformly in the embryo did not alter the activation profile (Fig. 1c). The activation profile at 18 °C was the same as that at 25 °C (Fig. 1d). This robustness to temperature variations is marked, considering the wide array of temperature dependencies that are observed in this temperature span. By contrast, the profile of pMad was sensitive to the concentration of Dpp[11] (Fig. 1d). The dosage sensitivity of Dpp is exceptional among morphogens and is singled out as being haploid-insufficient[12].

No apparent transcriptional feedback, which might account for the robustness of dorsal patterning, has been identified so far. Robustness should thus be reflected in the design of interactions in the patterning network. To identify the mechanism underlying robustness, we formulated a general mathematical model of the dorsal patterning network. For simplicity, our initial analysis was restricted to a single BMP class ligand (Scw or Dpp), a BMP inhibitor (Sog) and the protease (Tld). The general model accounted for the formation of the BMP–Sog complex, allowed for the diffusion of Sog, BMP and BMP–Sog, and allowed for the cleavage of Sog by Tld, both when Sog is free and when Sog is associated with BMP. Each reaction was characterized by a different rate constant. The three reaction–diffusion equations that define this model are given in the Methods.

We carried out extensive simulations to identify robust networks. At each simulation, a set of parameters (rate constants and protein

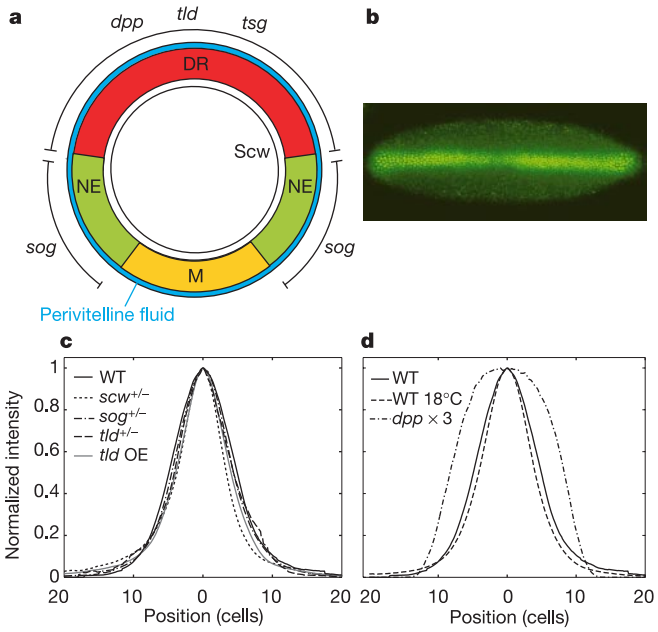

Figure 1 Robustness of the pMad activation profile. **a**, Cross-section of an early *Drosophila* embryo (~2 h after egg lay) showing the three distinct domains of gene expression. Starting at stage 5, the dorsal domain, which comprises about 50 cells, is subdivided to form the amnioserosa and the dorsal ectoderm. Shown are the genes of the patterning network: Scw and Dpp are two activating BMP class ligands; Sog is an inhibitor of both ligands; Tsg is required for Sog inhibition of Dpp; and Tld is a protease that cleaves Sog. Note that *dpp*, *tld* and *tsg* are expressed only in the dorsal region (DR), whereas expression of *sog* is restricted to the neuroectoderm (NE) and *scw* is expressed by all cells. M, mesoderm. **b**, Activation of the BMP pathway, which induces different cell fates in the dorsal region, visualized by antibodies against pMad. The activation profile is shown in a dorsal view of a wild-type embryo at stage 5. Activation is graded and peaks at the dorsal midline. The pattern of pMad widens at the termini of the embryo, possibly owing to edge effects that modify patterning. Our analysis is focused on the centre of the embryo, where the variability between different embryos is limited (~2 cells). **c**, Normalized activation profile of wild-type embryos (averaged over $n = 11$ embryos) compared with that of three sets of heterozygous mutants containing half the amount of Scw ($n = 23$), Sog ($n = 14$) and Tld ($n = 11$). The activation profile of embryos overexpressing the Tld protein uniformly around the embryo, using the Matα4–Gal4 driver, is also shown ($n = 33$). All embryos were collected at 25 °C. **d**, Activation profiles at 25 °C and 18 °C ($n = 41$). This temperature variation is biologically significant, as development is about two times slower at 18 °C than at 25 °C. Embryos were collected at different times but at the same developmental stage for the two temperatures. Shown also is the activation profile of an embryo carrying three copies of the *dpp* gene.

Box 1
Mechanism underlying robustness

We consider an idealized patterning network that consists of a single BMP (Scw for simplicity), Sog and Tld. Robustness will be manifested in the steady-state distribution of Scw. We assume that free Scw does not diffuse and that free Sog is not cleaved. The set of reaction–diffusion equations defining this network is obtained from equations 1–3 (Methods), by setting $D_{BMP} = \alpha_S = k_{-b} = 0$. At steady-state, the system can then be reduced to a single equation:

$$0 = \nabla^2([\mathrm{Scw}]^{-1}) - 2l_b^{-2} \quad (1)$$

where $l_b^2 = 2D_S/k_b$, D_S is the diffusion coefficient of Sog and k_b is the binding rate of Sog to Scw. Thus, although free Scw does not diffuse, the system is tuned for providing it with an effective diffusion. Two processes govern this effective diffusion: the shuttling of Scw by Sog from the circumference of the embryo into the dorsal midline, and the degradation of Sog by Tld in the dorsal region. Although both processes depend on the amounts of the respective proteins, those concentrations do not appear in the effective Scw diffusion. The key to this quantitative adjustment is the fact that both processes are mediated by the complex Sog–Scw: only the complex, and not free Scw, can diffuse, and only the complex is subject to degradation by Tld.

The concentrations of the network components, Scw, Sog and Tld could still affect the steady-state activation gradient through the boundary conditions. The solution of equation (1) is given by

$$[\mathrm{Scw}(x)] = \frac{l_b^2}{x^2 + \varepsilon^2} \quad (2)$$

where $x = 0$ at the dorsal midline and ε is an integration coefficient. In general, the value of ε will depend on most parameters of the system, including the concentrations and the production rates of the network components Scw, Sog and Tld, leading to a nonrobust distribution of Scw. Examining equation (2), however, we note that the only way to accommodate high concentrations of Scw is by placing Scw in a small region surrounding the dorsal midline where Sog is absent, in other words, by setting ε to 0. Thus, for large enough concentrations of Scw, ε vanishes and we obtain a robust Scw profile:

$$[\mathrm{Scw}(x)] = \frac{l_b^2}{x^2} \quad (3)$$

for every position of x that is far enough from the dorsal midline, in other words, $x \gg \varepsilon$. Indeed, the concentrations of network components have disappeared from this equation of the activation profile, which reflects the robustness of the system. Finally, we note that the same mechanism generates the gradient of the second BMP (Dpp). We assume, however, that Dpp binds Sog only when the latter is bound to Tsg. Thus, the same formalism is applied but with the molecular entities Dpp, Sog–Tsg (instead of Sog) and the complex Dpp–Sog–Tsg (instead of Scw–Sog). The details and precise conditions necessary for robustness are given in the Supplementary Information.

concentrations) was chosen at random and the steady-state activation profile was calculated by solving equations (1) to (3) numerically. A set of three perturbed networks representing heterozygous situations was then generated by reducing the gene dosages of *sog*, *tld* or the BMP class ligand by a factor of two. The steady-state activation profiles defined by those networks were solved numerically and compared with the initial, nonperturbed network. A threshold was defined as a given BMP value (corresponding to the value at a third of the dorsal ectoderm in the nonperturbed network). The extent of network robustness was quantified by measuring the shift in the threshold for all three perturbed networks. Over 66,000 simulations were carried out, with each of the nine parameters allowed to vary over four orders of magnitude.

As expected, in most cases (97.5%) the threshold position in the perturbed networks was shifted by a large extent (>50%; see Fig. 2a). In most of those nonrobust cases, the BMP concentration was roughly uniform throughout the dorsal region (Fig. 2c). By contrast, Sog was distributed in a concentration gradient with its minimum in the dorsal midline, defining a reciprocal gradient of BMP activation. Thus, the key event in this nonrobust patterning mechanism was the establishment of a concentration gradient of Sog, which was governed by diffusion of Sog from its domain of expression outside the dorsal region, coupled with its cleavage by Tld inside the dorsal region. Although such a gradient has been observed[13], it is also compatible with other models (see below).

We identified a small class of networks (198 networks, 0.3%) in which a twofold reduction in the amounts of all three genes resulted in a change of less than 10% in the threshold position (see Fig. 2b). Notably, in all of these robust cases, BMP was redistributed in a sharp concentration gradient that peaked in the dorsal midline (Fig. 2c). In addition, this concentration gradient decreased as a power-low distribution with an exponent $n = 2$, which indicated the uniqueness of the robust solution (Fig. 2d). In these cases, Sog was also distributed in a graded manner in the dorsal region (data not shown). Analysis of the reaction rate constants of the robust networks showed a wide range of possibilities for most parameters. But two restrictions were apparent and defined the robust network design. First, in the robust networks the cleavage of Sog by Tld was facilitated by the formation of the complex Sog–BMP (Fig. 2f). Second, the complex BMP–Sog was broadly diffusible, whereas free BMP was restricted (Fig. 2e).

To identify how robustness is achieved, we considered an idealized network by assuming that free Sog is not cleaved and that free BMP does not diffuse. The steady-state activation profile defined by this network can be solved analytically (Box 1), which reveals the two aspects that are crucial for ensuring robustness. First, the BMP–Sog complex has a central role, by coupling the two processes that establish the activation gradient: BMP diffusion and Sog degradation. This coupling leads to a quantitative buffering of perturbations in gene dosage. Second, restricted diffusion of free BMP enables the system to store excess BMP in a confined spatial domain where Sog is largely absent. Changes in the concentration of BMP

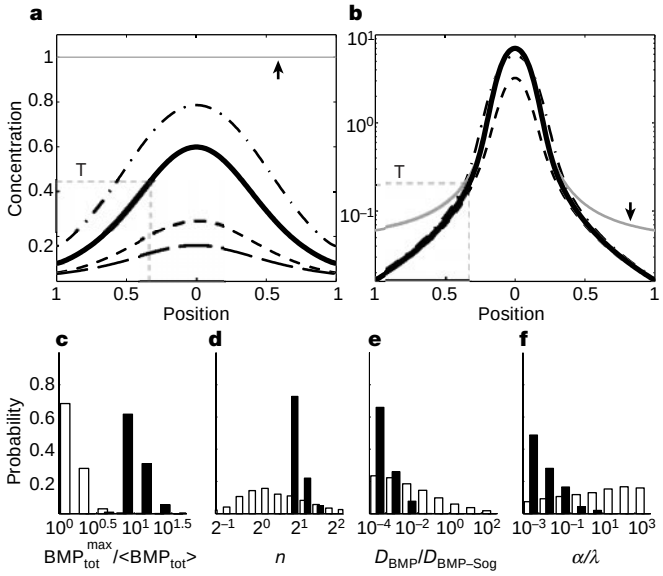

Figure 2 Patterning mechanism emerges from the features of the robust networks. The general model of the dorsal patterning network was solved numerically for 66,000 different choices of parameters, with each parameter ranging over four orders of magnitude. **a**, A typical, nonrobust network. The profile of free BMP (unbroken curves) is shown for the nonperturbed network and for three perturbed networks representing heterozygotes for *sog*, *tld* and BMP (see Fig. 1c for a key to the lines).The total concentration of BMP (free plus Sog-associated) is indicated by the grey line (arrow). The broken grey line (T) indicates the threshold where robustness was measured. **b**, A typical robust system. **c**–**f**, Statistical distribution of various features in the robust (black) and nonrobust (white) networks. The analysis was restricted to the 22,000 networks that showed at least twofold spatial variation of free BMP concentration. Each feature was calculated for each of the networks, and the histograms were normalized to account for the different numbers of robust (198) and nonrobust (22,000) networks. **c**, The extent of BMP confinement to the dorsal midline was quantified by measuring the ratio between total BMP concentration (free plus Sog-associated) at the centre and its average concentration. In all of the robust cases, a high ratio (>10) was observed. By contrast, the low ratios observed in the nonrobust cases indicated that BMP was distributed approximately uniformly. **d**, The steady-state profile of free BMP was fit to a power-low distribution, x^{-n}. Nearly all robust profiles corresponded to $n = 2$, indicating the uniqueness of the robust solution. By contrast, a wide range of exponents were found for the nonrobust solution. The fitting error vanished in the robust cases, but was high in the nonrobust cases (not shown). **e**, Ratio between the diffusion coefficient of free BMP (D_{BMP}) and the complex BMP–Sog ($D_{BMP-Sog}$). Note that complex formation significantly enhances BMP diffusion in all robust cases. **f**, Ratio of the degradation rate of free Sog (α) to that of BMP-associated Sog (λ). Note that complex formation greatly enhances Sog degradation in all robust cases.

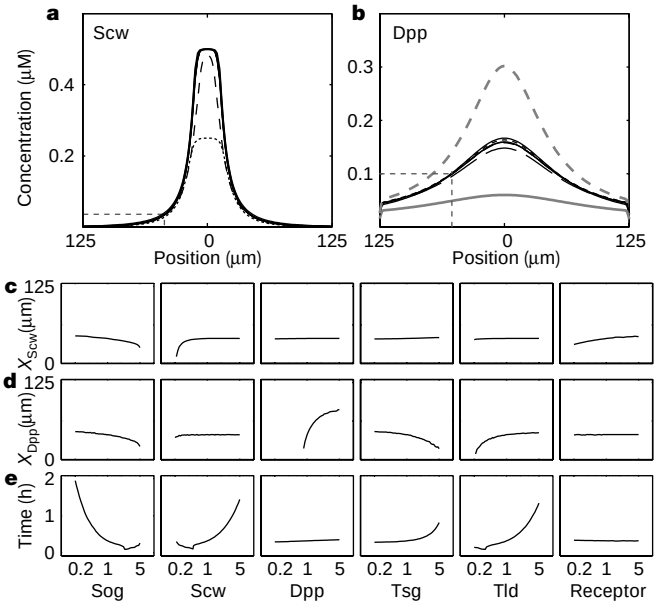

Figure 3 Properties of the robust model. **a**, **b**, The steady-state concentrations of receptor-bound Scw and Dpp. Six altered systems were obtained from a reference system by reducing to half the amounts of *scw*, *sog*, *tld* (see Fig. 1c for a key to the lines), *dpp* (unbroken grey line), Scw receptor (dotted line), *tsg* (superimposed on the solid line) and by increasing by 50% the amount of *dpp* (grey dashed line). The level and position of the threshold used in **c** and **d** are indicated. **c**, **d**, The positions of the activation thresholds of Scw (**c**) and Dpp (**d**) for a series of altered systems, obtained by changing a single parameter by the indicated fold amount. **e**, Time to reach steady state as a function of the fold change in parameter values. Time is initiated with the onset of ligand production.

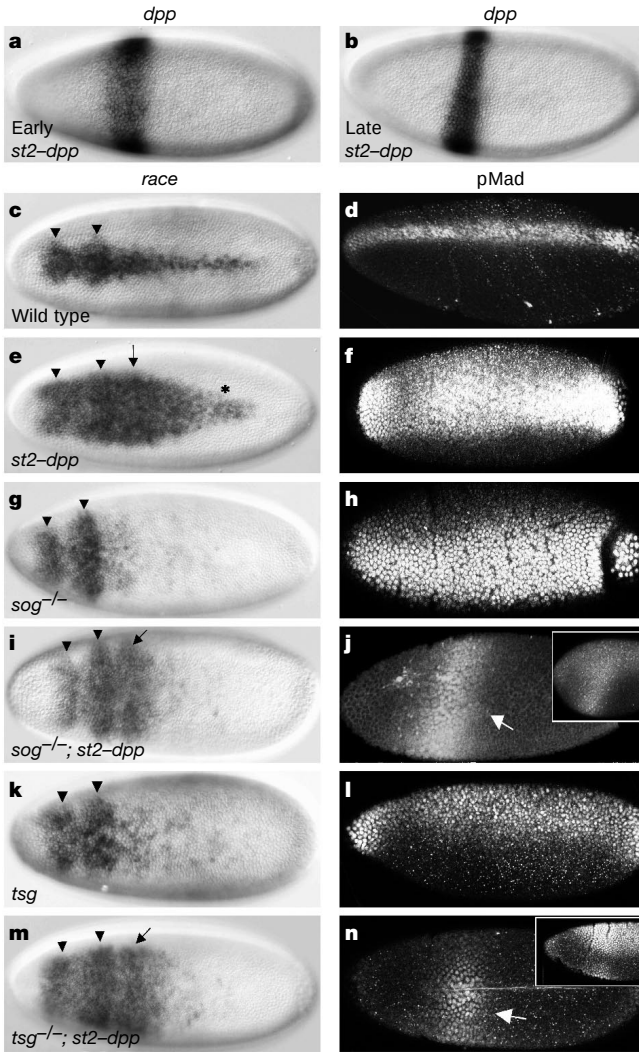

Figure 4 Dpp diffusion requires Sog and Tsg. Dpp was expressed orthogonal to the dorsoventral axis by the *eve st2* enhancer in a stripe of about 12 cells at early cleavage cycle 14 (**a**), which refines to about 6 cells by late cycle 14 (lateral views, **b**). Note that ectopic amounts of *dpp* were greater than the endogenous transcripts in the dorsal region, which under these exposures were not visible. **c**, Normal pattern of *race* in wild-type embryos. Note the AP bias in the anterior positions (arrowheads). **d**, Normal pattern of pMad in wild-type embryos. **e**, Expression of *st2–dpp* in wild-type embryos leads to an expanded expression of *race*, which forms a wedge shape with its broadest region at the position of *st2–dpp* (arrow) and ranges about 25 cells posteriorly (asterisk). The normal pattern of *race* shows an AP bias at the anterior positions (arrowheads). **f**, *st2–dpp* in wild-type embryos also leads to a broader dorsal distribution of pMad, which extends throughout the AP axis. **g**, In *sog* $^{-/-}$ embryos, the anterior *race* domain expands (arrowheads), whereas posterior expression is diminished and detected only sporadically as a punctate staining. Some expansion of *race* was observed in *sog* $^{+/-}$ embryos, probably due to the higher threshold of *race* induction compared with pMad. **h**, In *sog* $^{-/-}$ embryos, pMad expands in the dorsal domain, but does not reach the ventral domain. **i**, Expression of *st2–dpp* in *sog* $^{-/-}$ embryos leads to a corresponding stripe of *race* of about 10–12 cells (arrow). **j**, *st2–dpp* in *sog* $^{-/-}$ embryos generates a corresponding stripe of pMad (arrow), which extends to the ventral region. The ventral expansion of pMad versus the restricted dorsal expansion of *race* in embryos of the same genotype indicates that a lower threshold of activation can induce pMad even in the ventral domain, which is devoid of endogenous Dpp. Main view is ventral, inset is lateral. **k**, **l**, The patterns of *race* and pMad in *tsg* $^{-/-}$ embryos are similar to *sog* $^{-/-}$ embryos. **m**, **n**, *st2–dpp* in *tsg* $^{-/-}$ generates a corresponding stripe of both *race* and pMad, similar to that observed on expression of *st2–dpp* in *sog* $^{-/-}$ embryos. Main view in **n** is ventral, inset is lateral. Except where stated otherwise, a dorsal view is shown with anterior to the left.

alter the BMP profile close to the dorsal midline but do not change its distribution in most of the dorsal region (Box 1).

We next examined the complete system, comprising Sog, Tld, Tsg, both Scw and Dpp, and their associated receptors (Supplementary Information). Two additional molecular assumptions were required to ensure the robustness of patterning. First, Sog can bind and capture the BMP class ligands even when the latter are associated with their receptors. Second, Dpp can bind Sog only when the latter is bound to Tsg. Indeed, it has been shown that, whereas Sog is sufficient for inhibiting Scw, both Tsg and Sog are required for inhibiting Dpp[6,14,15]. This last assumption implies that Tsg functions to decouple the formation of the Scw gradient from the parallel generation of the Dpp gradient, ensuring that Scw and Dpp are transported to the dorsal midline independently by two distinct molecular entities (Supplementary Information).

The complete model was solved numerically for different choices of rate constants. In particular, we assessed the effect of twofold changes in gene dosage. The steady-state activation profiles can be superimposed, indicating the robustness of the system (Fig. 3a, b). In addition, with the exception of Dpp, the expression of all other crucial network components can be altered by at least an order of magnitude before an effect on the position of a given threshold is observed (Fig. 3c, d). In the model, the lack of robustness to Dpp stems from its insufficient dosage. Note that the time taken to reach steady state is sensitive to these concentrations of protein (Fig. 3e). For the wide range of parameters that we have used, however, the adjustment time does not exceed the patterning time. Flexible adjustment time thus facilitates the buffering of quantitative perturbations.

As discussed above, our analysis identified two principle molecular features that are essential for robust network design: first, free Sog is not cleaved efficiently—an assumption that is supported by the *in vitro* finding that Sog cleavage by Tld requires BMP[6,16]; second, the diffusion of free BMP is restricted. This is the central prediction of our theoretical study, namely, that Scw diffusion requires Sog, whereas Dpp diffusion requires both Sog and Tsg. Although several reports suggest that in wild-type embryos both Dpp and Scw are widely diffusible[6,17], their ability to diffuse in a *sog* or *tsg* mutant background has not been examined as yet.

To monitor the diffusion of Scw or Dpp, we used the *even-skipped* (*eve*) stripe-2 enhancer (*st2*) to misexpress Dpp or Scw in a narrow stripe perpendicular to the normal BMP gradient. In transgenic embryos, *dpp* or *scw* RNA was detected in a stripe just posterior to the cephalic furrow. Initially the stripe was about 12 cells wide at early cleavage cycle 14, but refined rapidly to about 6 cells by late cycle 14 (Fig. 4a, b). The *st2–dpp* and *st2–scw* embryos were viable, despite the high expression of these proteins as compared with their endogenous counterparts.

The activation of the BMP pathway was monitored either by staining for pMad or by following dorsal expression of the target gene *race*, which requires high activation. Scw is a less potent ligand than is Dpp. This experimental setup could not be used to study Scw diffusion properties because expressing *st2–scw* did not alter the pattern of pMad or *race* expression in wild-type or *sog* $^{-/-}$ embryos (data not shown). By contrast, expression of *st2–dpp* led to an expansion of both markers in a region that extends far from the *st2* expression domain, indicating a wide diffusion of Dpp in a wild-type background (compare Fig. 4c, d with 4e, f). Conversely, on expression of *st2–dpp* in *sog* $^{-/-}$ or in *tsg* $^{-/-}$ embryos, both markers were confined to a narrow stripe in the *st2* domain (compare Fig. 4g, h and k, l with 4i, j and m, n, respectively). The width of this stripe was comparable to that of *st2–dpp* expression, ranging from 6 to 12 cells, indicating that Dpp does not diffuse from its domain of expression in the absence of Sog or Tsg. Taken together, these results show that both Sog and Tsg are required for Dpp diffusion, as predicted by the theoretical analysis.

The computation ability of biochemical networks is striking when one considers that they function in a biological environment

where the amounts of the network components fluctuate, the kinetics is stochastic, and sensitive interactions between different computation modules are required. Studies have examined the effect of these properties on cellular computation mechanisms[18–20], and robustness has been proposed to be a 'design principle' of biochemical networks[18,21]. We have shown the applicability of this principle to morphogen gradient patterning during early development. Quantitative analysis can be used to assess rigorously the robustness of different patterning models and to exclude incompatible ones. The remaining, most plausible model points to crucial biological assumptions and serves to postulate the central feedback mechanisms. Applying the same modelling principles to other systems might identify additional 'design principles' that underlie robust patterning by morphogen gradients in development. □

Methods

Fly strains

We used the following strains: *screw*[12], *sog*[6], *tolloid*[2], *tolloid*[7], UAS–*tld* (provided by M. O'Connor), Matα4–Gal4 VP16 (provided by D. St. Johnston) and *tsg*^{XB56} (provided by L. Marsh). For altering the number of copies of *dpp*, we used the strain *dpp*^{1846} *sp cn bw/CyO 23P[dpp*$^{+}$*]* (provided by S. Roth), which was crossed to wild-type flies. The mutant chromosomes were maintained over a balancer chromosome. When each strain is crossed to itself, two-thirds of the embryos not showing the null phenotype should be heterozygotes for *scw* and *tld*, and a third for *sog*. The *st2–dpp* strain has been described[17]. We constructed *st2–scw* by inserting a *scw* cDNA fragment into plasmid 22FPE (ref. 22).

Antibodies and staining

Rabbit antibodies against pMad were kindly provided by P. ten Dijke. Freshly collected embryos were fixed in 7% formaldehyde. The remaining steps of staining were done according to standard procedures. We used Cy2-conjugated secondary antibodies against rabbit IgG (Jackson ImmunoResearch).

Data analysis

The dorso-ventral activation profile was quantified by using image processing tools written in Matlab. The mean intensity was measured at the middle of the anterior–posterior (AP) axis in a swath that was 20 cells wide in the direction of the AP axis. We then averaged the results over the indicated number of embryos.

Numerical simulations

For the general patterning model we considered a single BMP, which is denoted here as Scw. The model was defined by the following set of reaction–diffusion equations:

$$\frac{\partial[\mathrm{Sog}]}{\partial t} = D_{\mathrm{S}}\nabla^2[\mathrm{Sog}] - k_{\mathrm{b}}[\mathrm{Sog}][\mathrm{Scw}] + k_{-\mathrm{b}}[\mathrm{Sog{-}Scw}] - \alpha[\mathrm{Tld}][\mathrm{Sog}] \quad (1)$$

$$\frac{\partial[\mathrm{Scw}]}{\partial t} = D_{\mathrm{BMP}}\nabla^2[\mathrm{Scw}] - k_{\mathrm{b}}[\mathrm{Sog}][\mathrm{Scw}] + \lambda[\mathrm{Tld}][\mathrm{Sog{-}Scw}] + k_{-\mathrm{b}}[\mathrm{Sog{-}Scw}] \quad (2)$$

$$\frac{\partial[\mathrm{Sog{-}Scw}]}{\partial t} = D_{\mathrm{C}}\nabla^2[\mathrm{Sog{-}Scw}] + k_{\mathrm{b}}[\mathrm{Sog}][\mathrm{Scw}] - k_{-\mathrm{b}}[\mathrm{Sog{-}Scw}] - \lambda[\mathrm{Tld}] \times[\mathrm{Sog{-}Scw}] \quad (3)$$

The equations were solved in the region $-1 < x < 1$. The parameters in this model include the diffusion coefficients of Sog, Scw and the complex Scw–Sog, (D_{S}, D_{BMP} and D_{C}), binding and unbinding of the Scw–Sog complex (k_{b} and $k_{-\mathrm{b}}$), cleavage of Sog by Tld (α when Sog is free, λ when Sog in associated with Scw), a constant flux of Sog on the boundaries (η_{s}) and the total Scw concentration ($[\mathrm{Scw}]_{\mathrm{av}}$). D_{C} is $D_{\mathrm{BMP–Sog}}$ in Fig. 2e. We solved the equations for 66,000 different sets of random parameters. Each parameter was allowed to vary over four orders of magnitude. The parameters defining the centre of this distributions are (in arbitrary units): $D_{\mathrm{S}} = l_1 = [\mathrm{Scw}]_{\mathrm{av}} = 1$, $D_{\mathrm{BMP}} = 0.1$, $D_{\mathrm{C}} = 1$, $k_{\mathrm{b}} = 10$, $k_{-\mathrm{b}} = 1$, $\lambda[\mathrm{Tld}] = 10$, $\alpha[\mathrm{Tld}] = 10$, $\eta_{\mathrm{S}} = 10$. Equations were solved with Matlab. Each run took less than 1 min. The parameters of the systems shown in Fig. 2 are specified in the Supplementary Information.

For the parameters of the full model (Fig. 3), we chose diffusion rates that reflected the rapid *in vivo* patterning time and corresponded to the measured diffusion time in the perivitelline fluid[4]. This measured diffusion coefficient is similar to that of green fluorescent protein (GFP) in water[23]. It is possible that mixing processes in the perivitelline fluid contribute to the equilibration process. For simplicity, we approximate such processes as an effective diffusion. This approximation does not affect our conclusions. No biochemical data restricting the values of the other parameters are available. The parameters of the reference system are within the realistic biochemical range and obey the robustness conditions. The parameter choice is specified and rationalized in detail in the Supplementary Information.

Received 11 April; accepted 27 July 2002; doi:10.1038/nature01061.

1. Freeman, M. Feedback control of intercellular signalling in development. *Nature* **408,** 313–319 (2000).
2. Podos, S. D. & Ferguson, E. L. Morphogen gradients: new insights from DPP. *Trends. Genet.* **15,** 396–402 (1999).
3. Raftery, L. A. & Sutherland, D. J. TGF-β family signal transduction in *Drosophila* development: from Mad to Smads. *Dev. Biol.* **210,** 251–268 (1999).
4. Stein, D., Roth, S., Vogelsang, E. & Nusslein-Volhard, C. The polarity of the dorsoventral axis in the *Drosophila* embryo is defined by an extracellular signal. *Cell* **65,** 725–735 (1991).
5. DeRobertis, E. M. & Sasai, Y. A common plan for dorsoventral patterning in Bilateria. *Nature* **380,** 37–40 (1996).
6. Nguyen, M., Park, S., Marques, G. & Arora, K. Interpretation of a BMP activity gradient in *Drosophila* embryos depends on synergistic signaling by two type I receptors, SAX and TKV. *Cell* **95,** 495–506 (1998).
7. Arora, K., Levine, M. S. & O'Connor, M. B. The screw gene encodes a ubiquitously expressed member of the TGF-β family required for specification of dorsal cell fates in the *Drosophila* embryo. *Genes Dev.* **8,** 2588–2601 (1994).
8. Mason, E. D., Williams, S., Grotendorst, G. R. & Marsh, J. L. Combinatorial signaling by Twisted Gastrulation and Decapentaplegic. *Mech. Dev.* **64,** 61–75 (1997).
9. Persson, U. *et al.* The L45 loop in type I receptors for TGF-β family members is a critical determinant in specifying Smad isoform activation. *FEBS Lett.* **434,** 83–87 (1998).
10. Tanimoto, H., Itoh, S., ten Dijke, P. & Tabata, T. Hedgehog creates a gradient of DPP activity in *Drosophila* wing imaginal discs. *Mol. Cell* **5,** 59–71 (2000).
11. Dorfman, R. & Shilo, B.-Z. Biphasic activation of the BMP pathway in the *Drosophila* embryonic dorsal region. *Development* **128,** 965–972 (2001).
12. Wharton, K. A., Ray, R. P. & Gelbart, W. M. An activity gradient of decapentaplegic is necessary for the specification of dorsal pattern elements in the *Drosophila* embryo. *Development* **117,** 807–822 (1993).
13. Srinivasan, S., Rashka, K. E. & Bier, E. Creation of a Sog morphogen gradient in the *Drosophila* embryo. *Dev. Cell* **2,** 91–101 (2002).
14. Neul, J. L. & Ferguson, E. L. Spatially restricted activation of the SAX receptor by SCW modulates DPP/TKV signaling in *Drosophila* dorsal–ventral patterning. *Cell* **95,** 483–494 (1998).
15. Ross, J. J. *et al.* Twisted gastrulation is a conserved extracellular BMP antagonist. *Nature* **410,** 479–483 (2001).
16. Marques, G. *et al.* Production of a DPP activity gradient in the early *Drosophila* embryo through the opposing actions of the SOG and TLD proteins. *Cell* **91,** 417–426 (1997).
17. Ashe, H. L., Mannervik, M. & Levine, M. Dpp signaling thresholds in the dorsal ectoderm of the *Drosophila* embryo. *Development* **127,** 3305–3312 (2000).
18. Barkai, N. & Leibler, S. Robustness in simple biochemical networks. *Nature* **387,** 913–917 (1997).
19. Barkai, N. & Leibler, S. Circadian clocks limited by noise. *Nature* **403,** 267–268 (2000).
20. von Dassow, G., Meir, E., Munro, E. M. & Odell, G. M. The segment polarity network is a robust developmental module. *Nature* **406,** 188–192 (2000).
21. Hartwell, L. H., Hopfield, J. J., Leibler, S. & Murray, A. W. From molecular to modular biology. *Nature* **402,** C47–C52 (1999).
22. Kosman, D. & Small, S. Concentration-dependent patterning by an ectopic expression domain of the *Drosophila* gap gene *knirps*. *Development* **124,** 1343–1354 (1997).
23. Swaminathan, R., Hoang, C. P. & Verkman, A. S. Photobleaching recovery and anisotropy decay of green fluorescent protein GFP–S65T in solution and cells: cytoplasmic viscosity probed by green fluorescent protein translational and rotational diffusion. *Biophys. J.* **72,** 1900–1907 (1997).

Supplementary Information accompanies the paper on *Nature*'s website (http://www.nature.com/nature).

Acknowledgements

We thank P. ten Dijke for the pMad antibody; L. Marsh, M. O'Connor, S. Roth, D. St. Johnston and the Umea and Bloomington Fly Centers for strains; and S. Leibler and S. Roth for comments and criticism. This work was funded by the Israel Science Foundation (B-Z.S.) and the Israel Science Foundation and the Minerva Foundation (N.B). H.A. is a Lister Institute Research Fellow. B-Z.S. is the incumbent of the Hilda and Cecil Lewis professorial chair in Molecular Genetics. N.B. is the incumbent of the Soretta and Henry Shapiro career development chair.

Competing interests statement

The authors declare that they have no competing financial interests.

Correspondence and requests for materials should be addressed to N.B. (e-mail: naama.barkai@weizmann.ac.il).

Molecular basis of seasonal time measurement in *Arabidopsis*

Marcelo J. Yanovsky & Steve A. Kay

The Scripps Research Institute, 10550 N. Torrey Pines Road, La Jolla, California 92037, USA

Several organisms have evolved the ability to measure daylength, or photoperiod, allowing them to adjust their development in anticipation of annual seasonal changes. Daylength measurement requires the integration of temporal information, provided by the circadian system, with light/dark discrimination, initiated by specific photoreceptors. Here we demonstrate that in *Arabidopsis* this integration takes place at the level of CONSTANS

